Loss Mechanisms in Piezoelectrics: How to Measure Different Losses Separately

Kenji Uchino, *Member, IEEE*, and Seiji Hirose, *Member, IEEE*

***Abstract*—Losses in piezoelectrics are considered in general to have three different mechanisms: dielectric, mechanical, and piezoelectric losses. This paper deals with the phenomenology of losses first, then how to measure these losses separately in experiments. We found that heat generation at off-resonance is caused mainly by dielectric loss tan δ' (i.e., P-E hysteresis loss), not by mechanical loss, and that a significant decrease in mechanical Q_m with an increase of vibration level was observed in resonant piezoelectric ceramic devices, which is due to an increase in the extensive dielectric loss, not in the extensive mechanical loss. We propose the usage of the antiresonance mode rather than the conventional resonance mode, particularly for high power applications because the mechanical quality factor Q_B at an antiresonance frequency is larger than Q_A at a resonance frequency.**

I. Introduction

Loss or hysteresis in piezoelectrics exhibits both merits and demerits. For positioning actuator applications, hysteresis in the field-induced strain provides a serious problem and, for resonance actuation such as ultrasonic motors, loss generates significant heat in the piezoelectric materials. Further, in consideration of the resonant strain amplified in proportion to a mechanical quality factor, low (intensive) mechanical loss materials are preferred for ultrasonic motors. On the contrary, for force sensors and acoustic transducers, a low mechanical quality factor Q_m (which corresponds to high mechanical loss) is helpful to widen a frequency range for receiving signals.

Haerdtl [1] wrote a review article on electrical and mechanical losses in ferroelectric ceramics. Losses are considered to consist of four portions: domain wall motion; fundamental lattice portion, which also should occur in domain-free monocrystals; microstructure portion, which occurs typically in polycrystalline samples; and conductivity portion in highly ohmic samples. However, in the typical piezoelectric ceramic case, the loss due to the domain wall motion exceeds the other three contributions significantly. They reported interesting experimental results on the relationship between electrical and mechanical losses in piezoceramics, $Pb_{0.9}La_{0.1}(Zr_{0.5}Ti_{0.5})_{1-x}Me_xO_3$, where Me represents the doped ions Mn, Fe, or Al and x varied between 0 and 0.09. However, they measured the mechanical losses on poled ceramic samples, while the electrical losses on unpoled samples, i.e., in a different polarization state. Thus, they completely neglected piezoelectric losses.

As far as we know, not much research effort has been put into systematic studies of the loss mechanisms in piezoelectrics, particularly in high-voltage and high-power ranges. Because not many comprehensive descriptions can be found in previous reports, this paper will clarify the loss mechanisms in piezoelectrics phenomenologically, describe heat generation processes and high power characteristics, and discuss the resonance and antiresonance vibration modes from a viewpoint of a quality factor.

Although Ikeda [2] described part of the formulas of this paper in his textbook, he totally neglected the piezoelectric losses, which have been found not to be neglected in our investigations. We derive the full descriptions of the losses in this paper. It is also worth noting that we have changed the terminologies "extrinsic" and "intrinsic" losses used in our previous presentations and papers to "intensive" and "extensive" losses, respectively, in this paper.

II. Loss and Hysteresis in the Polarization Curve

A. Relation Between Hysteresis and Dissipation Factor

Let us start first with loss and hysteresis in the electric displacement D (nearly equal to polarization P) vs. electric field E curve without considering the electromechanical coupling. Fig. 1(a) shows an example of a P-E hysteresis curve. When the D (or P) traces a different line with increased and decreased applied electric field E, it is called hysteresis.

When the hysteresis is not very large, the electric displacement D can be expressed by using a slight phase lag to the applied electric field. The hysteresis curve shows an ellipse in this case. Assuming that the electric field oscillates at a frequency f(= $\omega/2\pi$) as

$$E^* = E_0 e^{j\omega t}, \tag{1}$$

the induced electric displacement also oscillates at the same frequency under the steady state, but with some time phase delay δ':

$$D^* = D_0 e^{j(\omega t - \delta')}. \tag{2}$$

Manuscript received May 19, 1999; accepted February 17, 2000. Part of this research was supported by the Office of Naval Research through grant no. N00014-96-1-1173 and N00014-99-1-0754.

K. Uchino is with the International Center for Actuators and Transducers, Materials Research Laboratory, The Pennsylvania State University, University Park, PA 16802 (e-mail: kenjiuchino@psu.edu).

S. Hirose is with the Faculty of Engineering, Yamagata University, Yonezawa 992, Japan.

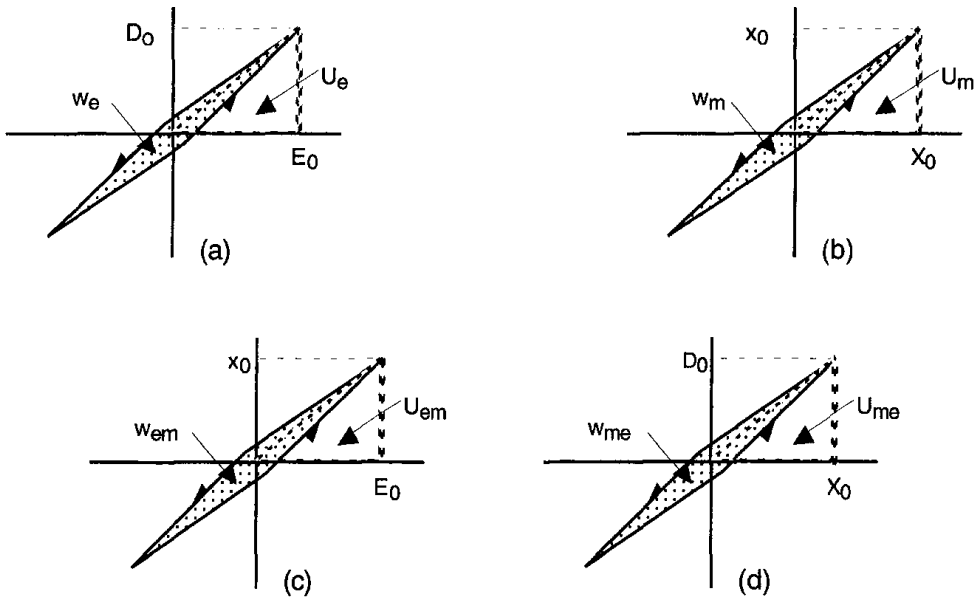

Fig. 1. (a) D vs. E (stress free), (b) x vs. X (short-circuit), (c) x vs. E (stress free), and (d) D vs. X (open-circuit) curves with a slight hysteresis in each relation.

If we express the relation between $D*$ and $E*$ as:

$$D^* = \varepsilon^* \varepsilon_0 E^*, \tag{3}$$

where the complex dielectric constant ε^* is:

$$\varepsilon^* = \varepsilon' - \mathrm{j}\varepsilon'', \tag{4}$$

and where

$$\varepsilon''/\varepsilon' = \tan\delta'. \tag{5}$$

Note that the negative connection in (4) comes from the time "delay," and that $\varepsilon'\varepsilon_0 = (D_0/E_0)\cos\delta'$ and $\varepsilon''\varepsilon_0 = (D_0/E_0)\sin\delta'$.

The area $\mathrm{w_e}$ corresponds to the consumed loss energy during an electric field cycle per unit volume of the dielectrics and can be related in isotropic dielectrics with ε'' or $\tan\delta'$ as follows:

$$\mathrm{w_e} = -\int \mathbf{D}\mathrm{d}\mathbf{E} = -\int_0^{2\pi/\omega} \mathbf{D}(\mathrm{d}\mathbf{E}/\mathrm{dt})\,\mathrm{dt} = \pi E_0 D_0 \sin\delta' = \pi\varepsilon''\varepsilon_0 E_0^2 = \pi\varepsilon'\varepsilon_0 E_0^2 \tan\delta'. \tag{6}$$

When there is no phase delay ($\delta' = 0$), $\mathrm{w_e} = 0$; i.e., the electrostatic energy stored in the dielectric will be recovered completely after a full cycle (100% efficiency). However, when there is a phase delay, the loss $\mathrm{w_e}$ will be accompanied per cycle, and the dielectric material generates heat. The $\tan\delta'$ is called dielectric dissipation factor.

In consideration of the stored electrostatic energy during a half cycle from $-E_0$ to E_0[$= 4\,\mathrm{U_e}$, which is illustrated as an area in Fig. 1(a)] provided by:

$$4\,\mathrm{U_e} = (1/2)(2\,E_0)(2\,\varepsilon'\varepsilon_0 E_0) = 2\,\varepsilon'\varepsilon_0 E_0^2, \tag{7}$$

the dissipation factor $\tan\delta'$ can be experimentally obtained by:

$$\tan\delta' = (1/2\pi)\,(\mathrm{w_e}/\mathrm{U_e}). \tag{8}$$

Note that $\mathrm{w_e}$ is the hysteresis in a full cycle and $\mathrm{U_e}$ is the stored energy in a quarter of a cycle.

B. Temperature, Electric Field, and Frequency Dependence of P-E Hysteresis

Fig. 2, 3, and 4 show temperature, electric field and frequency dependence of the dissipation factor $\tan\delta'$ calculated from the P-E hysteresis loss measured under stress-free conditions for a PZT-based ceramic. Experimental details are in [3]. The loss $\tan\delta'$ decreases gradually with increasing temperature, but it is rather insensitive to frequency. On the contrary, the $\tan\delta'$ increases initially in proportion to the applied electric field, exhibiting a saturation above a certain electric field. After reaching the saturation, i.e., more than 0.1 of $\tan\delta'$, this complex physical quantity treatment should not be used. The value for $E = 0$ (solid triangle mark in the figure) was obtained with an impedance analyzer.

III. General Consideration of Loss and Hysteresis

A. Theoretical Formulas

Let us expand the above discussion into more general cases, i.e., piezoelectric materials. We will start from the Gibbs free energy G expressed by:

$$\mathrm{dG} = -x\,\mathrm{d}X - D\,\mathrm{d}E - S\,\mathrm{d}T, \tag{9}$$

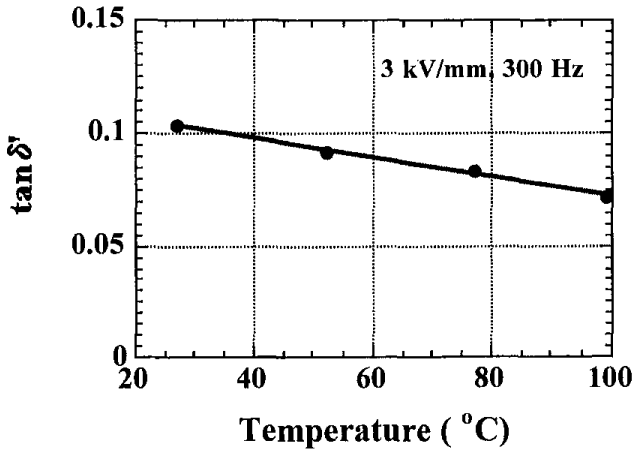

Fig. 2. Loss $\tan\delta'$ as a function of sample temperature (3 kV/mm, 300 Hz).

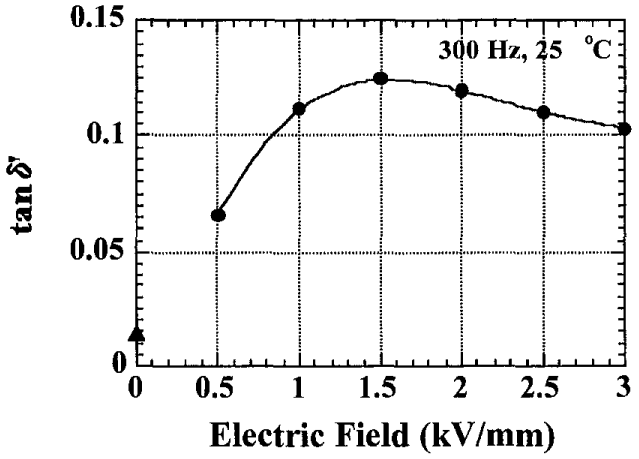

Fig. 3. Loss $\tan\delta'$ as a function of electric field (T = 25°C, f = 300 Hz).

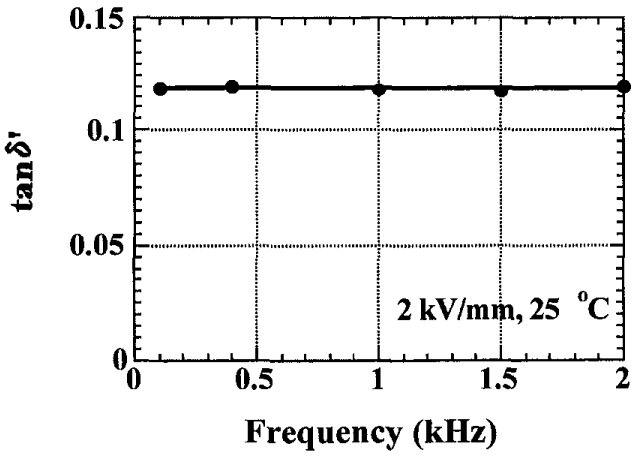

Fig. 4. Loss $\tan\delta'$ as a function of frequency (T = 25°C, E = 2 kV/mm).

or

$$G = -(1/2)\,s^E X^2 - d\,X\,E - (1/2)\,\varepsilon^x \varepsilon_0\,E^2. \tag{10}$$

Here, x is strain, X is stress, D is electric displacement, E is electric field, S is enthalpy, and T is temperature. (10) is the energy expression in terms of intensive (i.e., externally controllable) physical parameters X and E. Temperature dependence is carried into the elastic compliance s^E, the dielectric constant ε^X and the piezoelectric constant d. We will obtain the following two piezoelectric equations:

$$x = -(\partial G/\partial X) = s^E X + d\,E, \tag{11}$$

$$D = -(\partial G/\partial E) = d\,X + \varepsilon^X \varepsilon_0 E. \tag{12}$$

Note that thermodynamical equations and the consequent piezoelectric equations [(9)-(12)] cannot yield a delay-time-related loss without taking into account irreversible thermodynamic equations or dissipation functions, in general. However, the latter considerations are mathematically equivalent to the introduction of complex physical constants into the phenomenological equations, if the loss can be treated as a perturbation.

Therefore, we will introduce complex parameters ε^{X*}, s^{E*}, and d^* in order to consider the hysteresis losses in dielectric, elastic, and piezoelectric coupling energy:

$$\varepsilon^{X*} = \varepsilon^X(1 - j\tan\delta'), \tag{13}$$

$$s^{E*} = s^E(1 - j\tan\phi'), \tag{14}$$

$$d^* = d(1 - j\tan\theta'), \tag{15}$$

where θ' is the phase delay of the strain under an applied electric field, or the phase delay of the electric displacement under an applied stress. Both delay phases should be exactly the same if we introduce the same complex piezoelectric constant d^* into (11) and (12). δ' is the phase delay of the electric displacement to an applied electric field under a constant stress (e.g., zero stress) condition, and ϕ' is the phase delay of the strain to an applied stress under a constant electric field (e.g., short-circuit) condition. We will consider these phase delays as "intensive" losses.

Fig. 1(a)–(d) correspond to the model hysteresis curves for practical experiments: D vs. E curve under a stress-free condition, x vs. X under a short-circuit condition, x vs. E under a stress-free condition, and D vs. X under an open-circuit condition for measuring charge (or under a short-circuit condition for measuring current), respectively. Notice that these measurements are easily conducted in practice.

In a similar fashion to the previous section, the stored energies and hysteresis losses for pure dielectric and elastic energies can be calculated as:

$$U_e = (1/2)\varepsilon^X \varepsilon_0 E_0^2, \tag{16}$$

$$w_e = \pi \varepsilon^X \varepsilon_0 E_0^2 \tan\delta', \tag{17}$$

$$U_m = (1/2)\,s^E X_0^2, \tag{18}$$

$$w_m = \pi s^E X_0^2 \tan\phi'. \tag{19}$$

The electromechanical loss, when measuring the induced strain under an electric field, is more complicated. Let us calculate the stored energy U_{em} during a quarter electric field cycle (i.e., 0 to E_0) , first:

$$U_{em} = -\int x\,dX = (1/2)(x_0^2/s^E) = (1/2)(dE_0)^2/s^E = (1/2)(d^2/s^E)E_0^2. \quad (20)$$

Replacing d and s^E by $d^* = d(1 - j\tan\theta')$ and $s^{E^*} = s^E(1 - j\tan\phi')$, we obtain

$$U_{em} = (1/2)(d^2/s^E)E_0^2, \quad (21)$$

and

$$w_{em} = \pi(d^2/s^E)\,E_0^2\,(2\tan\theta' - \tan\phi'). \quad (22)$$

Note that the strain vs. electric field measurement seems to provide the piezoelectric loss $\tan\theta'$ directly; however, the observed loss should include an additional elastic loss because the strain should be delayed to the initial stress, which is needed to calculate energy.

Similarly, when we measure the induced charge under stress, the stored energy U_{me} and the hysteresis loss w_{me} during a quarter and a full-stress cycle, respectively, are obtained as:

$$U_{me} = (1/2)(d^2/\varepsilon_0\varepsilon^X)\,X_0^2, \quad (23)$$

and

$$w_{me} = \pi(d^2/\varepsilon_0\varepsilon^X)\,X_0^2\,(2\tan\theta' - \tan\delta'). \quad (24)$$

Hence, from the measurements of D vs. E and x vs. X, we obtain $\tan\delta'$ and $\tan\phi'$, respectively, and either the piezoelectric (D vs. X) or converse piezoelectric measurement (x vs. E) provides $\tan\theta'$ through a numerical subtraction.

So far, we have discussed the "intensive" dielectric, mechanical, and piezoelectric losses. In order to consider real physical meanings of the losses, we will introduce the "extensive" losses [2]. When we start from the energy expression in terms of extensive (material's own) physical parameters x and D, that is,

$$dA = X\,dx + E\,dD - S\,dT, \quad (25)$$

we can obtain the piezoelectric equations as follows:

$$X = (\partial A/\partial x) = c^D x - h\,D, \quad (26)$$

$$E = (\partial A/\partial D) = -h\,x + \kappa^x\kappa_0\,D. \quad (27)$$

We introduce the extensive dielectric, elastic, and piezoelectric losses as:

$$\kappa^{x^*} = \kappa^x(1 + j\tan\delta), \quad (28)$$

$$c^{D^*} = c^D(1 + j\tan\phi), \quad (29)$$

$$h^* = h(1 + j\tan\theta). \quad (30)$$

It is notable that the permittivity under a constant strain (e.g., zero strain or completely clamped) condition, ε^{x^*} and the elastic compliance under a constant electric displacement (e.g., open-circuit) condition, s^{D^*} can be provided as an inverse value of κ^{x^*} and c^{D^*}, respectively. Thus, using exactly the same losses in (28) and (29),

$$\varepsilon^{x^*} = \varepsilon^x(1 - j\tan\delta), \quad (31)$$

$$s^{D^*} = s^D(1 - j\tan\phi), \quad (32)$$

we will consider these phase delays again as "extensive" losses.

Here, we consider the physical property difference between the boundary conditions: E constant and D constant, or X constant and x constant. When an electric field is applied on a piezoelectric sample as illustrated in the top of Fig. 5, this state will be equivalent to the superposition of the following two steps; the sample is completely clamped and the field E_0 is applied (pure electrical energy $(1/2)\varepsilon^x\varepsilon_0 E_0^2$ is input); and keeping the field at E_0, the mechanical constraint is released (additional mechanical energy $(1/2)(d^2/s^E)\,E_0^2$ is necessary). The total energy should correspond to the total input electrical energy $(1/2)\varepsilon^X\varepsilon_0 E_0^2$; thus, we obtain the relation,

$$\varepsilon_0\varepsilon^X = \varepsilon_0\varepsilon^x + (d^2/s^E). \quad (33)$$

Similarly, from the bottom of Fig. 5,

$$s^E = s^D + (d^2/\varepsilon_0\varepsilon^X). \quad (34)$$

Hence, we obtain the following equations:

$$\varepsilon^x/\varepsilon^X = (1 - k^2), \quad (35)$$

$$s^D/s^E = (1 - k^2), \quad (36)$$

where

$$k^2 = d^2/(s^E\,\varepsilon_0\varepsilon^X). \quad (37)$$

Similarly,

$$\kappa^X/\kappa^x = (1 - k^2), \quad (38)$$

$$c^E/c^D = (1 - k^2), \quad (39)$$

where

$$k^2 = h^2/(c^D\,\kappa^x\kappa_0). \quad (40)$$

This k is called the electromechanical coupling factor, and is the same as the k in (37), because the equation $d^2/(s^E\varepsilon_0\varepsilon^X) = h^2/(c^D\,\kappa^x\kappa_0)$ can be verified mathematically. We define the k as a real number in this manuscript.

In order to obtain the relationships between the intensive and extensive losses, the following three equations are essential:

$$\varepsilon_0\varepsilon^X = [\kappa^x\kappa_0\,(1 - h^2/(c^D\,\kappa^x\kappa_0))]^{-1}, \quad (41)$$

$$s^E = [c^D\,(1 - h^2/(c^D\,\kappa^x\kappa_0))]^{-1}, \quad (42)$$

$$d = [h^2/(c^D\,\kappa^x\kappa_0)]\,[h\,(1 - h^2/(c^D\,\kappa^x\kappa_0))]^{-1}. \quad (43)$$

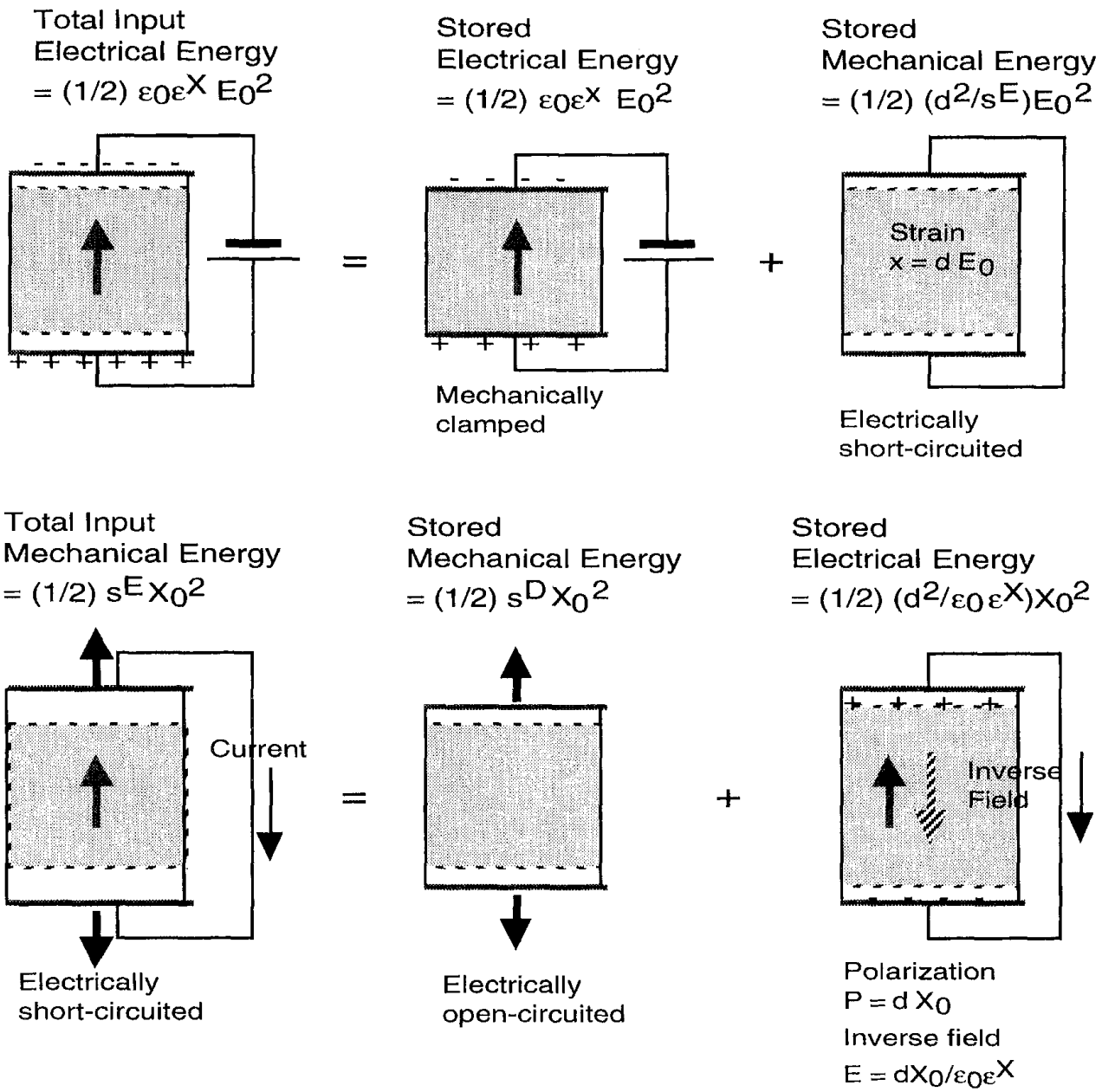

Fig. 5. Conceptual figure for explaining the relation between ε^{X} and ε^{x}, s^{E}, and s^{D}.

Replacing the parameters in (41) (43) by the complex parameters in (13) (15), (28)–(30), we obtain the relationships between the intensive and extensive losses:

$$\tan\delta' = (1/(1-k^2))[\tan\delta + k^2(\tan\phi - 2\tan\theta)], \tag{44}$$

$$\tan\phi' = (1/(1-k^2))[\tan\phi + k^2(\tan\delta - 2\tan\theta)], \tag{45}$$

$$\tan\theta' = (1/(1-k^2))[\tan\delta + \tan\phi - (1+k^2)\tan\theta], \tag{46}$$

where k is the electromechanical coupling factor defined by either (37) or (40), and here as a real number. It is important that the intensive dielectric and elastic losses are mutually correlated with the extensive dielectric, elastic, and piezoelectric losses through the electromechanical coupling k^2, and that the denominator $(1-k^2)$ comes basically from the ratios, $\varepsilon^{x}/\varepsilon^{X} = (1-k^2)$ and $s^{D}/s^{E} = (1-k^2)$, and this real part reflects to the dissipation factor when the imaginary part is divided by the real part. Also note that, depending on the vibration mode, the definition of electromechanical coupling k can be changed such as $k^2 = d^2/(s^{D}\varepsilon_0\varepsilon^{X})$.

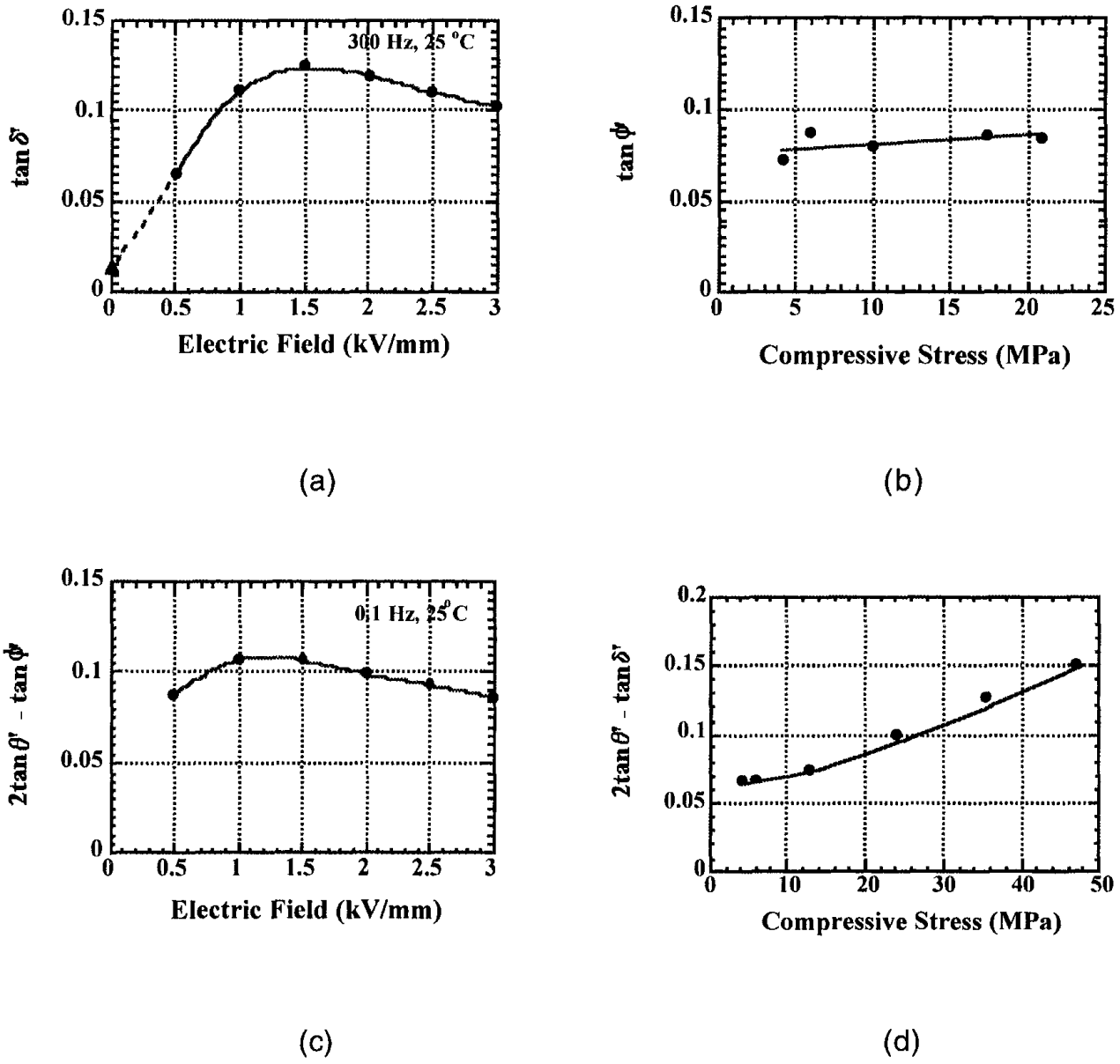

Fig. 6. Dissipation factors determined from (a) D vs. E (stress free), (b) x vs. X (short-circuit), (c) x vs. E (stress free), and (d) D vs. X (open-circuit) curves for a PZT-based actuator.

B. Experimental Example

Fig. 6 shows "intensive" dissipation factors determined from Fig. 6(a) D vs. E (stress free), Fig. 6(b) x vs. X (short-circuit), Fig. 6(c) x vs. E (stress free), and Fig. 6(d) D vs. X (open-circuit) curves for a soft PZT-based multilayer actuator used for Figs. 2, 3, and 4. The details on the experiments will be reported in the successive papers. Fig. 7 shows the result for the piezoelectric loss $\tan\theta'$. We used the correlation factor between electric field and compressive stress given averagely by $X = (\varepsilon_0 \varepsilon^{\mathrm{X}}/s^{\mathrm{E}})^{1/2} E$.

From Figs. 6 and 7, we can calculate the "extensive" losses as shown in Fig. 8. Note that the piezoelectric losses $\tan\theta'$ and $\tan\theta$ are not as small as previously believed, but they are comparable to the dielectric and elastic losses and increase gradually with the field or stress. Also it is noteworthy that the extensive dielectric loss $\tan\delta$ increases significantly with an increase of the intensive parameter (i.e., the applied electric field), and the extensive elastic loss $\tan\phi$ is rather insensitive to the intensive parameter, i.e., the applied compressive stress.

When similar measurements to Figs. 1(a) and (b), but under constrained conditions—that is, D vs. E, under a completely clamped state, and x vs. X, under an open-circuit state, respectively—we can expect smaller hystereses, that is, extensive losses, $\tan\delta$ and $\tan\phi$. These mea-

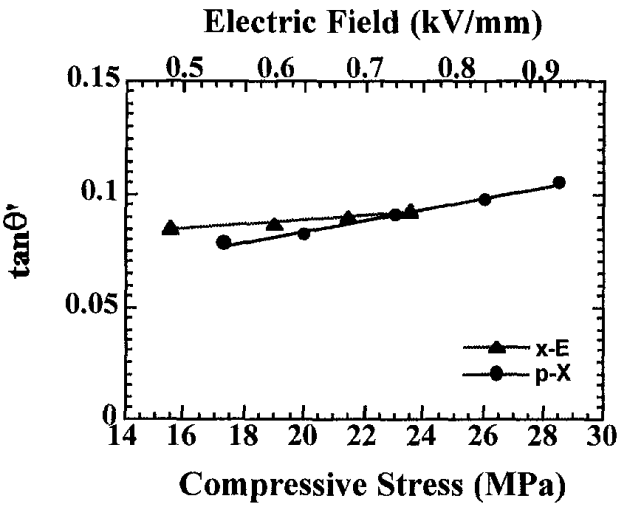

Fig. 7. Extrinsic piezoelectric dissipation factor $\tan\theta'$ as a function of electric field or compressive stress, measured for a PZT-based actuator.

surements seem to be alternative methods to determine the three losses separately; however, they are rather difficult in practice.

IV. Loss and Heat Generation

Heat generation in various types of PZT-based actuators has been studied under a relatively large electric field applied (1 kV/mm or more) at an off-resonance frequency, and a simple analytical method was established to evaluate the temperature rise, which is very useful for the design of piezoelectric high-power actuators. Heat generation in a resonating piezoelectric sample is discussed in the next section.

Zheng *et al.* [3] reported the heat generation from various sizes of multilayer type piezoelectric ceramic actuators. Fig. 9 shows the temperature change with time in the actuators when driven at 3 kV/mm and 300 Hz. Fig. 10 plots the saturated temperature as a function of V_c/A, where V_e is the effective volume (electrode overlapped part) and A is the surface area. This linear relation is reasonable because the volume V_c generates the heat, and this heat is dissipated through the area A. Thus, if we need to suppress the temperature rise, a small V_e/A design is preferred.

According to the law of energy conservation, the rate of heat storage in the piezoelectric resulting from heat generation and dissipation effects can be expressed as:

$$q_g - q_{out} = V\rho c\,(dT/dt), \tag{47}$$

assuming uniform temperature distribution in the sample. V, ρ, c are total volume, density, and specific heat, respectively. The heat generation is considered to be caused by losses. Thus, the rate of heat generation (q_g) in the piezoelectric can be expressed as:

$$q_g = u\,f\,V_e, \tag{48}$$

where u is the loss of the sample per driving cycle per unit volume, f is the driving frequency, and V_e is the effective volume where the ceramic is activated. According to the measuring condition, this u corresponds to the intensive dielectric loss w_e of (17), which consists of the extensive dielectric loss $\tan\delta$ and the electromechanical and piezoelectric combined loss $(\tan\phi - 2\tan\theta)$ in the previous section:

$$\begin{aligned} u = w_e &= \pi\varepsilon^X\varepsilon_0 E_0^2 \tan\delta' \\ &= [1/(1-k^2)][\tan\delta + k^2(\tan\phi - 2\tan\theta)]\pi\varepsilon^X\varepsilon_0 E_0^2. \end{aligned} \tag{49}$$

Note that we do not need to add w_{em} explicitly, because the corresponding electromechanical loss is already included implicitly in w_e.

When we neglect the conduction heat transfer, the rate of heat dissipation (q_{out}) from the sample is the sum of the rates of heat flow by radiation (q_r) and convection (q_c):

$$\begin{aligned} q_{out} &= q_r + q_c \\ &= \sigma e A(T^4 - T_0^4) + h_c A(T - T_0), \end{aligned} \tag{50}$$

where σ is the Stefan-Boltzmann constant, e is the emissivity of the sample, h_c is the average convective heat transfer coefficient, and A is the sample surface area. Thus, (47) can be written in the form:

$$u\ f\ V - A\ k(T)(T - T_0) = V\rho c(dT/dt), \tag{51}$$

where

$$k(T) = \sigma e(T^2 + T_0^2)(T + T_0) + h_c \tag{52}$$

is defined as the overall heat transfer coefficient. If we assume that $k(T)$ is relatively insensitive to temperature change, the solution to (51) for the piezoelectric sample temperature is given as a function of time (t):

$$T - T_0 = [u\ f\ V_e/k(T)\,A]\,[1 - e^{-t/\tau}], \tag{53}$$

where the time constant τ is expressed as:

$$\tau = \rho c V/k(T)A. \tag{54}$$

As $t \to \infty$, the maximum temperature rise in the sample becomes:

$$\Delta T = u\ f\ V_e/k(T)\,A. \tag{55}$$

As $t \to 0$, the initial rate of temperature rise is:

$$(dT/dt) = u\ f\ V_e/\rho c\ V = \Delta T/\tau. \tag{56}$$

Figs. 11 and 12 show the dependence of $k(T)$ on applied electric field and frequency. Because $k(T)$ is not really constant, we can calculate the total loss u of the piezoelectric

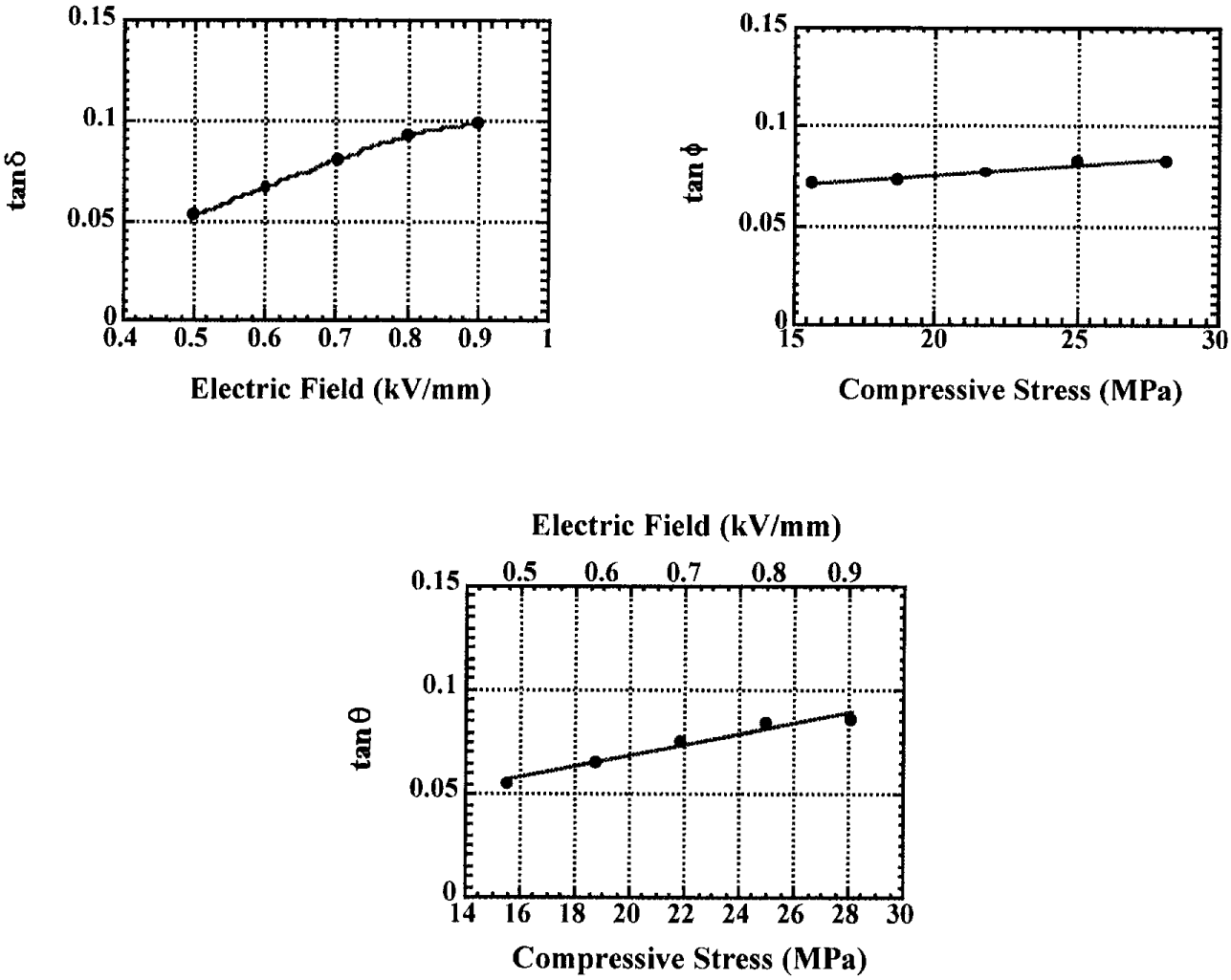

Fig. 8. Intrinsic loss factors $\tan\delta$, $\tan\phi$, and $\tan\theta$ as a function of electric field or compressive stress, measured for a PZT-based actuator.

more precisely through (56). The calculated results are shown in Table I. The experimental data of P-E hysteresis losses under a stress-free condition also are listed for comparison. It is seen that the P-E hysteresis intensive loss agrees well with the total loss contributing to the heat generation under an off-resonance drive.

V. Losses at a Piezoelectric Resonance

So far, we have considered the losses for a quasi-static or off-resonance state. Problems in ultrasonic motors that are driven at the resonance frequency include significant distortion of the admittance frequency spectrum due to nonlinear behavior of elastic compliance at a high vibration amplitude, and heat generation that causes a serious degradation of the motor characteristics through depoling of the piezoceramic. Therefore, the ultrasonic motor requires a very hard-type piezoelectric with a high mechanical quality factor Q_m, leading to the suppression of heat generation. It is also notable that the actual mechanical vibration amplitude at the resonance frequency is directly proportional to this Q_m value.

A. Losses at a Piezoelectric Resonance

1. Piezoelectric Resonance Without Loss: Let us first review the longitudinal mechanical vibration of a piezoceramic plate without loss through the transverse piezoelectric effect (d_{31}) as shown in Fig. 13 [4]. Assuming that the polarization is in the z-direction and the x-y planes are the planes of the electrodes, the extentional vibration in the x direction is represented by the following dynamic equation:

$$\rho(\partial^2 u/\partial t^2) = F = (\partial X_{11}/\partial x) + (\partial X_{12}/\partial y) + (\partial X_{13}/\partial z), \tag{57}$$

where u is the displacement of the small volume element in the ceramic plate in the x-direction and ρ is the density. When the plate is very long and thin, X_2 and X_3 may be

TABLE I
LOSS AND OVERALL HEAT TRANSFER COEFFICIENT FOR PZT MULTILAYER SAMPLES ($E = 3$ kV/mm, f = 300 Hz).

Actuator	4.5 × 3.5 × 2 mm	7 × 7 × 2 mm	17 × 3.5 × 1 mm
Total loss ($\times 10^3$J/m^3)			
$u = \frac{\rho cv}{fv_e}\left(\frac{dT}{dt}\right)_{t\to 0}$	19.2	19.9	19.7
$P-E$ hysteresis loss ($\times 10^3$J/m^3)	18.5	17.8	17.4
k(T) (W/m^{2}K)	38.4	39.2	34.1

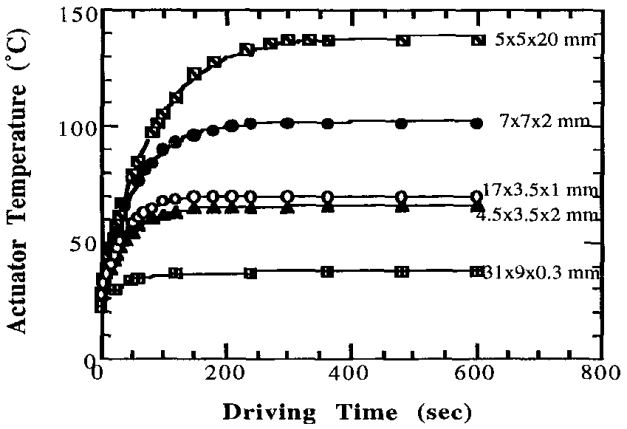

Fig. 9. Temperature rise for various actuators while driven at 300 Hz and 3 kV/mm.

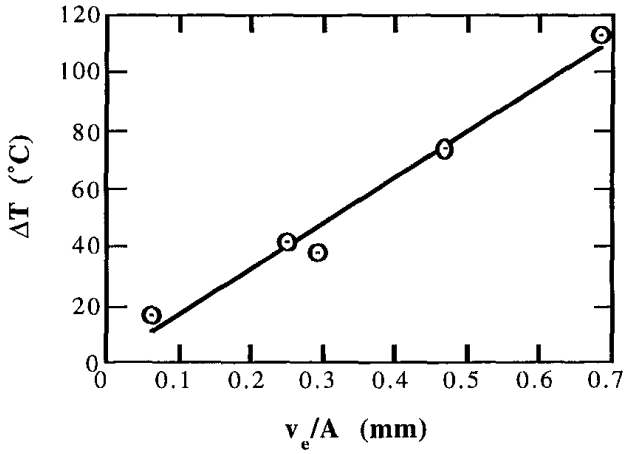

Fig. 10. Temperature rise vs. V_e/A (3 kV/mm, 300 Hz), where V_e is the effective volume generating the heat and A is the surface area dissipating the heat.

set equal to zero through the plate, and the relation between stress, electric field (only E_z exists), and the induced strain is given by:

$$X_1 = x_1/s_{11}^E - (d_{31}/s_{11}^E)E_z. \tag{58}$$

Introducing (58) into (57) and allowing for $x_1 = \partial u/\partial x$ and $\partial E_z/\partial x = 0$ (due to the equal potential on each electrode), leads to a harmonic vibration equation:

$$-\omega^2 \rho s_{11}^E u = \partial^2 u/\partial x^2. \tag{59}$$

Here, ω is the angular frequency of the drive field. Substituting a general solution $u = u_1(x)e^{j\omega t} + u_2(x)e^{-j\omega t}$ into (58), and with the boundary condition $X_1 = 0$ at x = 0 and L (sample length), a solution can be obtained as shown in (60) and (61) (top of next page). Here, v is the sound velocity in the piezoceramic, which is given by:

$$v = 1/\sqrt{\rho s_{11}^E}. \tag{62}$$

Because the total current is given by (63) (top of next page) and using (60), the admittance for the mechanically free sample is calculated to be (64) (top of next page), where w is the width, L is the length, t is the thickness of the sample, and V is the applied voltage. ε_3^{LC} is the permittivity in a longitudinally clamped sample, which is given by:

$$\varepsilon_0\varepsilon_3^{LC} = \varepsilon_0\varepsilon_3^X - (d_{31}^2/s_{11}^E) = \varepsilon_0\varepsilon_3^X(1 - k_{31}^2). \tag{65}$$

The final transformation is provided by the definition,

$$k_{31} = d_{31}/\sqrt{s_{11}^e \varepsilon_0 \varepsilon_3^X}. \tag{66}$$

When the drive frequency is much lower than the resonance, taking $\omega \to 0$ (64) leads to $Y = (j\omega wL/t)\varepsilon_3^X$ (corresponding to the static capacitance). The piezoelectric resonance is achieved when the admittance becomes infinite or the impedance is zero. The resonance frequency f_R is calculated from (64), and the fundamental f_R is given by:

$$f_R = v/2L = 1/\left(2L\sqrt{\rho s_{11}^E}\right). \tag{67}$$

However, the antiresonance state is generated for zero admittance or infinite impedance:

$$(\omega_A L/2v)\cot(\omega_A L/2v) = -d_{31}^2/\varepsilon_3^{LC}s_{11}^E = -k_{31}^2/\left(1 - k_{31}^2\right). \tag{68}$$

The resonance and antiresonance states are described by the following intuitive model [4]. In a high electromechanical coupling material with k almost equal to 1, the resonance or antiresonance states appear for $\tan(\omega L/2v) = \infty$ or 0 [i. e., $\omega L/2v = (m - 1/2)\pi$ or $m\pi$ (m: integer)], respectively. The strain amplitude x_1 distribution for each state [calculated using (60)] is illustrated in Fig. 14. In the

$$\text{(strain)} \quad \partial u/\partial \mathrm{x} = x_1 = \mathrm{d}_{31} E_z [\sin \omega(\mathrm{L} - \mathrm{x})/\mathrm{v} + \sin(\omega \mathrm{x}/\mathrm{v})]/\sin(\omega \mathrm{L}/\mathrm{v}), \tag{60}$$

$$\text{(total displacement)} \quad \Delta \mathrm{L} = \int_0^{\mathrm{L}} x_1 \mathrm{dx} = \mathrm{d}_{31} E_z \mathrm{L}(2\mathrm{v}/\omega \mathrm{L}) \tan(\omega \mathrm{L}/2\mathrm{v}) \tag{61}$$

$$i = \mathrm{j}\omega \mathrm{w} \int_0^{\mathrm{L}} D_3 \, \mathrm{dx} = \mathrm{j}\omega \mathrm{w} \int_0^{\mathrm{L}} \left[\left(\varepsilon_0 \varepsilon_3^{\mathrm{x}} - \mathrm{d}_{31}^2/\mathrm{s}_{11}^{\mathrm{E}} \right) E_z + (\mathrm{d}_{31}/\mathrm{s}_{11}^{\mathrm{E}}) x_1 \right] \mathrm{dx}, \tag{63}$$

$$\begin{aligned} \mathrm{Y} &= (1/\mathrm{Z}) = (i/V) = (i/E_z \mathrm{t}) \\ &= (\mathrm{j}\omega \mathrm{wL}/\mathrm{t}) \varepsilon_0 \varepsilon_3^{\mathrm{LC}} \left[1 + (\mathrm{d}_{31}^2/\varepsilon_0 \varepsilon_3^{\mathrm{LC}} \mathrm{s}_{11}^{\mathrm{E}}) (\tan(\omega \mathrm{L}/2\mathrm{v})/(\omega \mathrm{L}/2\mathrm{v})) \right], \end{aligned} \tag{64}$$

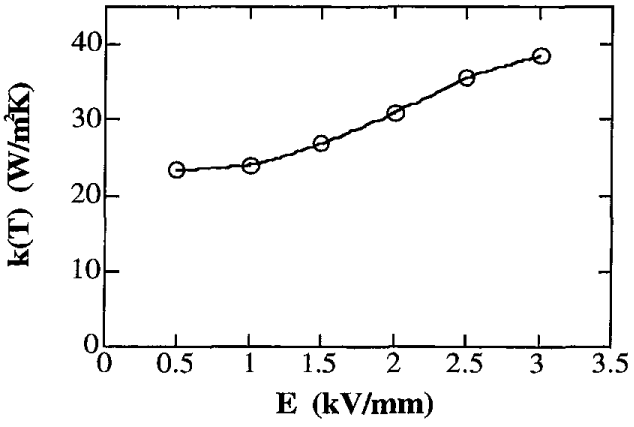

Fig. 11. $k(T)$ as a function of applied electric field (400 Hz, data from the actuator with dimensions of 7 mm × 7 mm × 2 mm).

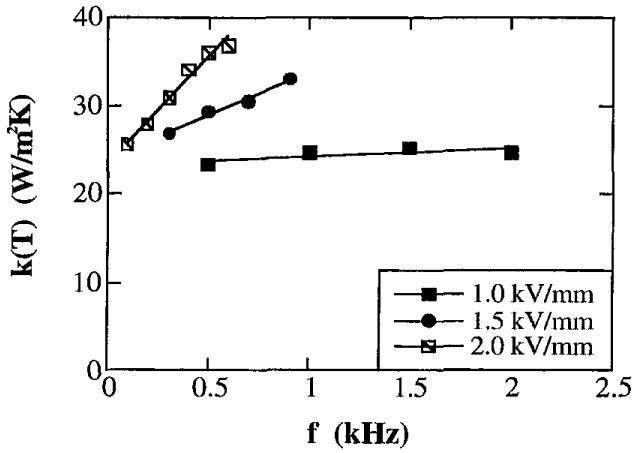

Fig. 12. Overall heat transfer coefficient k(T) as a function of frequency.

resonance state, large strain amplitudes and large capacitance changes (called motional capacitance) are induced, and the current can easily flow into the device. Note that, for a loss-free piezoelectric, the strain is calculated to be infinite in (60). However, at the antiresonance, the strains induced in the device cancel each other completely, resulting in no capacitance change, and the current cannot flow easily into the sample. Both ends of the plate correspond to the nodal points, which do not generate any motion to be used for actuators. Thus, for a high k material, the first antiresonance frequency $\mathrm{f_A}$ should be twice as large as the first resonance frequency $\mathrm{f_R}$.

In a typical case, where $\mathrm{k_{31}} = 0.3$, the antiresonance state varies from the above-mentioned mode and becomes closer to the resonance mode. The low-coupling mate-

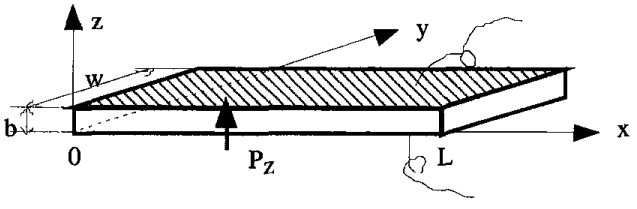

Fig. 13. Longitudinal vibration through the transverse piezoelectric effect ($\mathrm{d_{31}}$) in a rectangular plate.

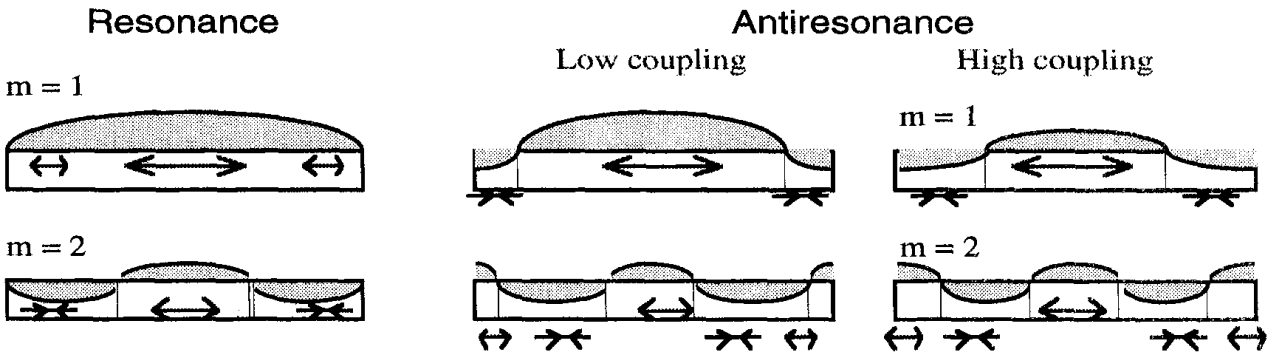

Fig. 14. Strain generation in the resonance or antiresonance state. The strain magnitude is plotted in the vertical axis as a function of the x coordinate.

rial exhibits an antiresonance mode in which capacitance change due to the size change is compensated completely by the current required to charge up the static capacitance (called damped capacitance). Thus, the antiresonance frequency f_A will approach the resonance f_R.

When $(f_A - f_R)$ is not very large due to a small electromechanical coupling, we can derive the following approximate expression for f_A. Assuming that $\omega_A - \omega_R$ is much smaller than $\omega_R (= \pi v/L)$, and

$$(\omega_A L/2v)\cot[(\omega_A - \omega_R)L/2v - \pi/2] = -k_{31}^2/\left(1 - k_{31}^2\right). \tag{69}$$

Thus,

$$\omega_A = (\pi v/L)[1 + (4/\pi^2)K_{31}^2], \tag{70}$$

where we introduced a new parameter K_{31} as:

$$K_{31}^2 = k_{31}^2/(1 - k_{31}^2). \tag{71}$$

It is notable that, for a piezoelectric sample with a typical k_{31} value, the two ends of the plate are not the nodal points; that is, we can expect rather large displacements, which can be applied for ultrasonic motors.

2. Piezoelectric Resonance with Losses: Now we will introduce the complex parameters into the admittance curve around the resonance frequency, in a similar way to the previous section: $\varepsilon_3^{X*} = \varepsilon_3^X(1 - j\tan\delta')$, $s_{11}^{E*} = s_{11}^E(1 - j\tan\phi')$, and $d_{31}^* = d(1 - j\tan\theta')$ into (64) [see (72); next page]. For (72),

$$C_0 = (wL/t)\varepsilon_0\varepsilon_3^X, \tag{73}$$

$$C_d = (1 - k_{31}^2)C_0. \tag{74}$$

Note that the loss for the first term (damped conductance) is represented by the "extensive" dielectric loss $\tan\delta$, not by the intensive loss $\tan\delta'$. Taking into account

$$v^* = 1/\sqrt{\rho s_{11}^E(1 - j\tan\phi')} = v(1 + (1/2)j\tan\phi'), \tag{75}$$

we further calculate $1/\tan(\omega L/2v^*)$ with an expansion-series approximation around $(\omega L/2v) = \pi/2$. The resonance state is defined in this case for the maximum admittance point, rather than the infinite Y.

We will use new frequency parameters,

$$\Omega = \omega L/2v, \Delta\Omega = \Omega - \pi/2 (\ll 1). \tag{76}$$

Because $\omega L/2v^* = (\pi/2 + \Delta\Omega)[1 - (1/2)j\tan\phi']$,

$$1/\tan(\omega L/2v^*) = -\Delta\Omega + j(\pi/4)\tan\phi'. \tag{77}$$

Thus, using $K_{31}^2 = k_{31}^2/(1 - k_{31}^2)$, the motional admittance Y_m is approximated around the first resonance frequency by (78) (top of next page). The maximum Y_m is obtained at $\Delta\Omega = 0$:

$$Y_m^{max} = (8/\pi^2)\omega_0 C_d K_{31}^2(\tan\phi')^{-1}. \tag{79}$$

In order to obtain the mechanical quality factor, let us obtain $\Delta\Omega$, which provides $Y_m^{max}/\sqrt{2}$. Because $\Delta\Omega = (\pi/4)\tan\phi'$ is obtained,

$$Q_m = \Omega_0/2\Delta\Omega = (\pi/2)/2(\pi/4)\tan\phi' = (\tan\phi')^{-1}. \tag{80}$$

This verifies the already used relation, $Q_m = (\tan\phi')^{-1}$.

Here, the displacement amplification also is considered. From (61), also by using the complex parameters, (81) is true (see top of next page). The maximum displacement u_{max} is obtained at $\Delta\Omega = 0$:

$$u_{max} = (8/\pi^2)d_{31}E_z L(\tan\phi')^{-1}. \tag{82}$$

The maximum displacement at the resonance frequency is $(8/\pi^2)$ Q_m times larger than that at a nonresonance frequency $(d_{31}E_z L)$.

In a brief summary, we obtained an already used knowledge: when we observe the admittance or displacement spectrum as a function of drive frequency, and obtain the mechanical quality factor Q_m estimated from $Q_m = \omega_0/2\Delta\omega$, where $2\Delta\omega$ is a full width of the 3 dB down (i.e., $1/\sqrt{2}$) of the maximum value at $\omega = \omega_0$, we can obtain the intensive mechanical loss $\tan\phi'$.

B. Equivalent Circuit

The equivalent circuit for the piezoelectric actuator is represented by a combination of L, C, and R. Fig. 15(a)

$$
\begin{aligned}
Y &= Y_d + Y_m \\
&= (j\omega wL/t)\varepsilon_0\varepsilon_3^X(1-k_{31}^2)[1-j\,(1/(1-k_{31}^2))(\tan\delta' + k_{31}^2(\tan\phi' - 2\tan\theta'))] \\
&+ (j\omega wL/t)\varepsilon_0\varepsilon_3^X k_{31}^2[1-j(2\tan\theta' - \tan\phi')][\tan(\omega L/2\,v^*)/(\omega L/2v^*)] \\
&= j\omega C_0(1-k_{31}^2)[1-j(1/(1-k_{31}^2))(\tan\delta' + k_{31}^2(\tan\phi' - 2\tan\theta'))] \\
&+ j\omega C_0 k_{31}^2[1-j(2\tan\theta' - \tan\phi')][\tan(\omega L/2v^*)/(\omega L/2v^*)] \\
&= j\omega C_d(1-j\tan\delta) + j\omega C_d K_{31}^2[1-j(2\tan\theta' - \tan\phi')][\tan(\omega L/2v^*)/(\omega L/2v^*)], \qquad (72)
\end{aligned}
$$

$$
\begin{aligned}
Y_m &= j\omega C_d\, K_{31}^2[1-j(2\tan\theta' - \tan\phi')][\tan(\omega L/2v*)/(\omega L/2v^*)] \\
&= j\omega_0 C_d\, K_{31}^2[1-j(2\tan\theta' - \tan\phi')]/[(-\Delta\Omega + j(\pi/4)\tan\phi')(\pi/2)(1-(1/2)j\tan\phi')] \\
&= j(8/\pi^2)\omega_0 C_d\, K_{31}^2[(1+j(3/2)\tan\phi' - 2\tan\theta')]/[(-(4/\pi)\Delta\Omega + j\tan\phi')]. \qquad (78)
\end{aligned}
$$

$$
\begin{aligned}
u(L) &= d_{31}^* E_z L(2v^*/\omega L)\tan(\omega L/2v^*) \\
&= 2d_{31}(1-j\tan\theta')\,E_z L[v(1+(1/2)\,j\tan\phi')/\omega L]\,\tan(\omega L/2v^*) \\
&= 2d_{31}(1-j\tan\theta')\,E_z L[v(1+(1/2)\,j\tan\phi')/\omega_0 L]/(-\Delta\Omega + j(\pi/4)\tan\phi'). \qquad (81)
\end{aligned}
$$

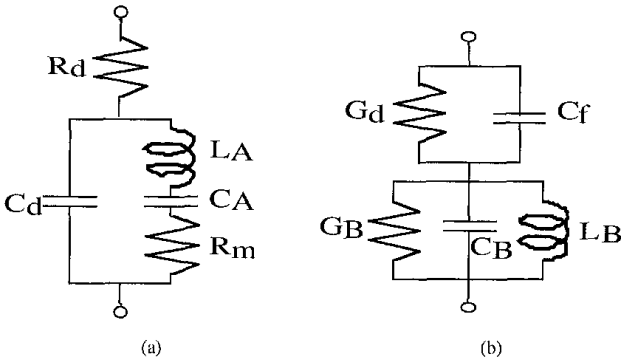

Fig. 15. Equivalent circuit of a piezoelectric device for the resonance (a) and the antiresonance (b).

shows an equivalent circuit for the resonance state, which has very low impedance. Taking into account (72), we can understand that C_d and R_d correspond to the electrostatic capacitance (for a longitudinally clamped sample in the previous case, not a free sample) and the clamped (or "extensive") dielectric loss $\tan\delta$, respectively, and the components L_A and C_A in a series resonance circuit are related to the piezoelectric motion. For example, in the case of the longitudinal vibration of the above rectangular plate through d_{31}, these components are represented approximately by

$$L_A = (\rho/8)(Lb/w)(s_{11}^{E2}/d_{31}^2), \qquad (83)$$

$$C_A = (8/\pi^2)(Lw/b)(d_{31}^2/s_{11}^E). \qquad (84)$$

The total resistance $R_A(=R_d+R_m)$ should correspond to the loss $\tan\phi'$, which is composed of the extensive mechanical loss $\tan\phi$ and dielectric/piezoelectric coupled loss $(\tan\delta - 2\tan\theta)$ (45). Thus, intuitively speaking, R_d and R_m correspond to the extensive dielectric and mechanical losses, respectively. Note that we introduced an additional resistance R_d to explain a large contribution of the dielectric loss when a vibration velocity is relatively large. Precisely speaking, the above description is not very true. The details will be reported in a forthcoming paper. In contrast, the equivalent circuit for the antiresonance state of the same actuator is shown in Fig. 15(b), which has high impedance.

C. Losses as a Function of Vibration Velocity

Fig. 16 shows the mechanical Q_m vs. basic composition x at two effective vibration velocities $v_0 = 0.05$ m/s and 0.5 m/s for $Pb(Zr_xTi_{1-x})O_3$ doped with 2.1 at.% of Fe [5]. The decrease in mechanical Q_m with an increase of vibration level is minimum around the rhombohedral-tetragonal morphotropic phase boundary (52/48). In other words, the smallest Q_m material at a small vibration level becomes the best at a large vibration level, and the data obtained by a conventional impedance analyzer with a small voltage/power does not provide data relevant to high power materials.

Let us consider the degradation mechanism of the mechanical quality factor Q_m with increasing vibration velocity. Fig. 17 shows an important notion on heat generation from the piezoelectric material [6]. The damped and mo-

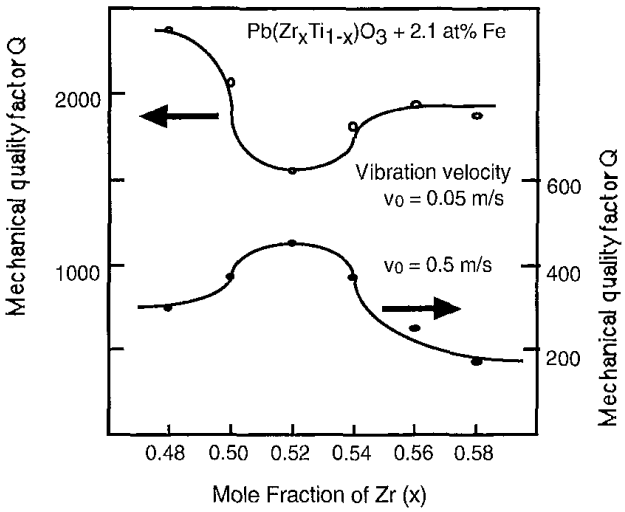

Fig. 16. Mechanical Q_m versus basic composition x at two effective vibration velocities $v_0 = 0.05$ m/s and 0.5 m/s for $Pb(Zr_xTi_{1-x})O_3$ doped with 2.1 at.% of Fe.

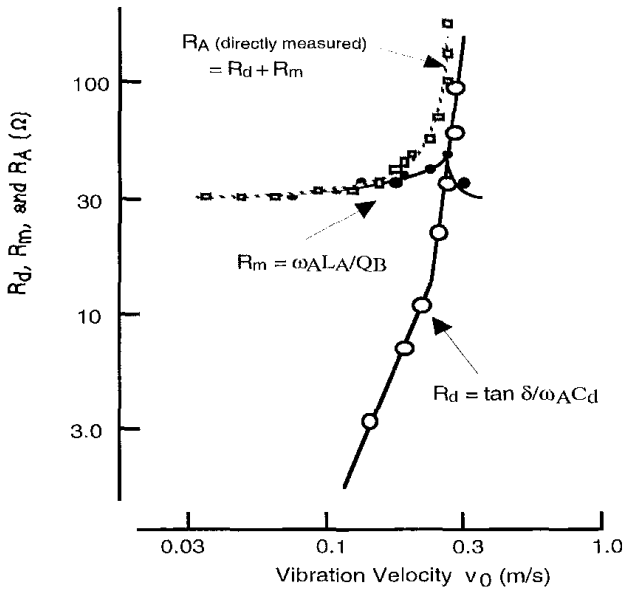

Fig. 17. Vibration velocity dependence of the resistances R_d and R_m in the equivalent electric circuit for a PZT sample.

tional resistances, R_d and R_m, in the equivalent electrical circuit of a PZT sample are separately plotted as a function of vibration velocity. Note that R_m, mainly related to the extensive mechanical loss, is insensitive to the vibration velocity; and R_d, related to the extensive dielectric loss, increases significantly around a certain critical vibration velocity. Thus, the resonance loss at a small vibration velocity is mainly determined by the extensive mechanical loss which provides a high mechanical quality factor Q_m, and with increasing vibration velocity, the extensive dielectric loss contribution significantly increases. After R_d exceeds R_m, we started to observe heat generation.

Tashiro *et al.* [7] observed the heat generation in a rectangular piezoelectric plate during a resonating drive. Even though the maximum electric filed is not very large, heat is generated due to the large induced strain/stress at the resonance. The maximum heat generation was observed at the nodal point of the resonance vibration, at which the maximum strain/stress are generated. This observation supports that the heat generation in a resonating sample is attributed to the intensive elastic loss $\tan\phi'$. This is not contradictory to the result in Section IV, in which a high-voltage was applied at an off-resonance frequency. We concluded there that the heat is originated from the intensive dielectric loss $\tan\delta'$. In consideration that both the "intensive" dielectric and mechanical losses are composed of the "extensive" dielectric and mechanical losses, and that the extensive dielectric loss $\tan\delta$ changes significantly with the external electric field and stress, the major contribution to the heat generation seems to come from the "extensive" dielectric loss. Further investigations are needed for the microscopic explanations of this phenomenon.

VI. Losses at Resonance and Antiresonance Modes

A. Losses at a Piezoelectric Antiresonance State

We consider here the losses at the antiresonance frequency in comparison with the resonance mode. The antiresonance mode is obtained at a frequency that provides the minimum value of admittance Y, instead of zero of Y for the loss-free case. Taking an approximation technique on (72) around the antiresonance frequency ω_A, similar to the previous section, we obtain:

$$\Omega_A = \omega_A L/2v, \Delta\Omega = \Omega - \Omega_A (\ll 1). \tag{85}$$

If k_{31} is not very large, the following relationship is obtained:

$$\Omega_A = \omega_A L/2v = (\pi/2)(1 + (4/\pi^2)\, k_{31}^2). \tag{86}$$

In the following approximation, however, this relation is not used; but we will neglect the higher order of $\Delta\Omega$ and $\tan\phi'$ in (72), yielding (87) (top of next page). Taking into account (88) and (89) (top of next page), where

$$K_{31}^2 = k_{31}^2/(1 - k_{31}^2). \tag{90}$$

Then, Y^{min} can be obtained at $\Delta\Omega = 0$:

$$Y^{min} = \omega C_d (1/2) \tan\phi' (\Omega_A^2 + K_{31}^2 + K_{31}^4)/K_{31}^2. \tag{91}$$

$\sqrt{2}\, Y^{min}$ can be obtained at:

$$\Delta\Omega = (1/2)\, \Omega_A \tan\phi'. \tag{92}$$

$$Y = j\omega C_d \left\{1 + (k_{31}^2/(1-k_{31}^2))\tan[(\Omega_A + \Delta\Omega)(1 - j(1/2)\tan\phi')]/ [(\Omega_A + \Delta\Omega)(1 - j(1/2)\tan\phi')]. \right. \quad (87)$$

$$\tan[(\Omega_A + \Delta\Omega)(1 - j(1/2)\tan\phi')] = [(\Omega_A^2 - K_{31}^2\Delta\Omega + j(1/2)\Omega_A \tan\phi' K_{31}^2]/[(-K_{31}^2 - \Omega_A\Delta\Omega) - j\Omega_A(1/2)\Omega_A \tan\phi'], \quad (88)$$

$$Y = j\omega C_d(\Omega_A^2 + K_{31}^2 + K_{31}^4)[-\Delta\Omega + j(1/2)\Omega_A \tan\phi']/ [-K_{31}^2\Omega_A - (\Omega_A^2 + K_{31}^2)\Delta\Omega + j(1/2)\Omega_A \tan\phi'(\Omega_A^2 + K_{31}^2)], \quad (89)$$

Thus, mechanical quality factor at the antiresonance can be obtained as:

$$Q_m = \Omega_A/2\Delta\Omega = (\tan\phi\prime)^{-1}. \quad (93)$$

Q_m at the antiresonance could be verified to be equal to Q_m at the resonance ($= (\tan\phi')^{-1}$) in the first approximation neglecting the higher order terms more than $(\Delta\Omega)^2$, $(\tan\phi')^2$ etc. However, this result shows a discrepancy with the experimental results as discussed below. Further higher order approximation analysis will be required.

B. Experimental Results

Fig. 18 illustrates mechanical quality factors, Q_A, Q_B and the temperature rise for the resonance (A-type) and the antiresonance (B-type) modes for a rectangular-shaped hard PZT resonator plotted as a function of vibration velocity [6]. The sample size is indicated in Fig. 18 (43 mm × 7 mm × 2 mm). Note that an "effective" vibration velocity v_0 is a material's constant independent of the sample size, and it is defined as $\sqrt{2}\pi f u_{max}$ where f is the resonance or antiresonance frequency and u_{max} is the maximum vibration amplitude of the piezoelectric device [8]. Again it is noteworthy that the mechanical quality factor decreases significantly above a certain critical vibration velocity (0.1 m/s), at which a steep temperature rise starts. We have suggested that the heat generation is mainly attributed to the extensive dielectric loss rather than the mechanical loss. Note also that Q_B is higher than Q_A over the entire vibration velocity range, and that the temperature rise of the sample is less for the B-type resonance (antiresonance) than for the A-type resonance for the same vibration level. This indicates an intriguing idea that the antiresonance mode should be superior to the conventional resonance mode, particularly for high-power applications such as ultrasonic motors. In a typical piezoelectric material with k_{31} around 30%, the plate edge is not a vibration nodal point and can generate a large vibration velocity.

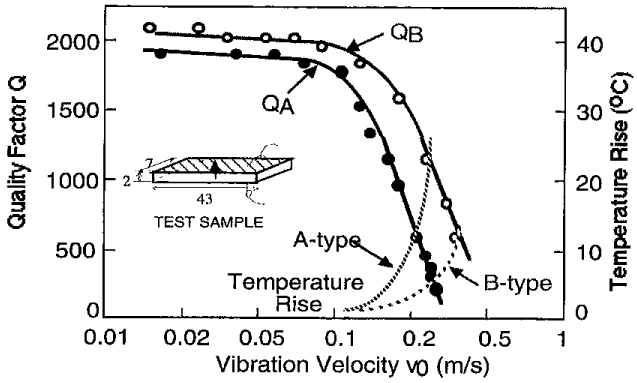

Fig. 18. Vibration velocity dependence of the quality factor Q (Q_A, Q_B) and temperature rise for both A (resonance) and B (antiresonance) type resonances of a longitudinally vibrating PZT ceramic transducer through the transverse piezoelectric effect d_{31}.

VII. Conclusions

Various techniques for measuring the electric, mechanical, and piezoelectric coupling losses separately have been discussed:

- D vs. E, x vs. X, x vs. E and D vs. X curves for dielectric, mechanical, and piezoelectric losses,
- heat generation at a resonance or an off-resonance frequency for an intensive mechanical or dielectric loss,
- resonance/antiresonance technique for intensive and extensive mechanical losses, respectively.

By combining the above methods, we can investigate the loss mechanisms in practical piezoelectric materials.

The piezoelectric losses $\tan\theta'$ and $\tan\theta$ are not as small as previously believed, but they are comparable to the dielectric and elastic losses in soft PZTs. Also, it is noteworthy that the extensive dielectric loss $\tan\delta$ increases significantly with an increase of the intensive parameter, i.e., the applied electric field; and the extensive elastic loss $\tan\phi$ is rather insensitive to the intensive parameter, i.e., the applied compressive stress.

Heat generation is caused mainly by the intensive dielectric loss $\tan\delta'$ (i.e., P-E hysteresis loss) for an off-resonance state under a high-drive, electric field, and by the intensive mechanical loss $\tan\phi'$ for a resonance state. Both situations are attributed to the large "extensive dielectric loss" enhanced by a large external electric field or stress. In order to suppress the temperature rise practically, a transducer design with larger surface area is recommended (for example, a tube rather than a rod).

A significant decrease in mechanical Q_m with an increase of vibration level was observed in resonant piezoelectric ceramic devices, and the data obtained by a conventional impedance analyzer with a small voltage/power do not provide data relevant to high-power materials.

Because the mechanical quality factor Q_B at an antiresonance frequency is larger than Q_A at a resonance frequency, the antiresonance mode seems to be superior to the conventional usage of the resonance mode, particularly for high-power applications such as ultrasonic motors.

Because the above conclusions were derived from only a limited number of PZT-based soft and hard piezoelectrics, it is too early to generalize these conclusions. Further investigations are highly required.

References

[1] K. H. Haerdtl, *Ceram. Int.*, vol. 8, pp. 121–127, 1982.

[2] T. Ikeda, *Fundamentals of Piezoelectric Materials Science*. Tokyo: Ohm Publication, 1984, p. 83.

[3] J. Zheng, S. Takahashi, S. Yoshikawa, K. Uchino, and J.W.C. de Vries, *J. Amer. Ceram. Soc.*, vol. 79, pp. 3193–3198, 1996.

[4] K. Uchino, *Piezoelectric Actuators and Ultrasonic Motors*. Boston: Kluwer, 1997, p. 197.

[5] S. Takahashi and S. Hirose, *Jpn. J. Appl. Phys.*, vol. 32, pp. 2422–2425, 1993.

[6] S. Hirose, M. Aoyagi, Y. Tomikawa, S. Takahashi, and K. Uchino, *Proc. Ultrason.*, Edinburgh, 1995, pp. 184–187.

[7] S. Tashiro, M. Ikehiro, and H. Igarashi, *Jpn. J. Appl. Phys.*, vol. 36, pp. 3004–3009, 1997.

[8] K. Uchino, J. Zheng, A. Joshi, Y. H. Chen, S. Yoshikawa, S. Hirose, S. Takahashi, and J.W.C. de Vries, *J. Electroceram.*, vol. 2, pp. 33–40, 1998.

Kenji Uchino (M'89), one of the pioneers in piezoelectric actuators, is the Director of International Center for Actuators and Transducers and Professor of Electrical Engineering at The Pennsylvania State University.

After being awarded his Ph.D. degree from Tokyo Institute of Technology, Japan, Uchino became a research associate in the Physical Electronics Department at this Institute. He then joined the Sophia University, Japan, as an associate professor in physics in 1985. He moved to Penn State in 1991. He also was involved with the Space Shuttle Utilizing Committee in NASDA, Japan, during 1986–1988, and he was the Vice President of NF Electronic Instruments during 1992–1994. He is the Chairman of the Smart Actuator/Sensor Study Committee, sponsored by Japanese MITI. He is also the executive associate editor for the *Journal of Advanced Performance Materials* (Kluwer Academic) and the associate editor of the *Journal of Intelligent Materials Systems and Structures* (Technomic), and the *Japanese Journal of Applied Physics*.

His research interests are in solid state physics, especially dielectrics, ferroelectrics, and piezoelectrics, including basic research on materials, device designing, and fabrication processes, as well as development of solid state actuators for precision positioners, ultrasonic motors, etc. He has authored 270 papers, 31 books, and has 16 patents in the ceramic actuator area.

He is a recipient of the Outstanding Research Award from Penn State Engineering Society (1996), Academic Scholarship from Nissan Motors Scientific Foundation (1990), Best Movie Memorial Award at Japan Scientific Movie Festival (1989), and the Best Paper Award from the Japanese Society of Oil/Air Pressure Control (1987). He also is a Fellow of the American Ceramic Society and a member of the IEEE.

Seiji Hirose received the B.S. degree in electronics in 1971 from Yamagata University, Yonezawa, Japan, and the Ph.D. degree in 1989 from Tohoku University, Sendai, Japan. Since April 1971, he has been with the Yamagata University, Yonezawa, Japan, where he is a professor of electronics and information engineering.

His research interest is in the high-power characteristics of the piezoelectric material and the piezoelectric transformer.

Dr. Hirose is a member of the Acoustical Society of Japan, the Material Society of America, and IEEE.